International Journal of
Nanoscience and Nanotechnology

Research Article

2025, Volume 21, Issue 3

Magnetohydrodynamic Flow and Heat Transfer Enhancement with Al_2O_3-Cu Hybrid Ionanofluids over an Exponentially Stretching/ Shrinking Permeable Sheet with Heat Generation and Slip Effect

Abanti Datta[1*], Arka Banerjee[2], Sayantan Mukherjee[3]

Received 25 July 2025
Accepted 10 September 2025

DOI: 10.22034/ijnn.2025.2066935.2685

International Journal of Nanoscience and Nanotechnology

Abstract

Effective heat transfer fluids are pivotal for high-performance thermal management systems. Although conventional nanofluids exhibit improved thermal properties, their practical applications are often hindered by agglomeration and flow instability. To overcome these challenges, this study investigates a hybrid ionanofluid, comprising Al_2O_3 and Cu nanoparticles dispersed in a water–$[C_2mim][CH_3SO_3]$ ionic liquid mixture under magnetohydrodynamic (MHD) boundary-layer (BL) flow conditions. The study focuses on analyzing how magnetic field strength, heat generation, suction, velocity and thermal slip influence the flow and heat transfer characteristics over an exponentially stretching or shrinking permeable surface. The governing partial differential equations are transformed via similarity variables and solved using MATLAB bvp4c solver. A linear stability analysis is performed to distinguish the physically realizable solution branch in cases of dual solutions. The results demonstrate that the hybrid ionanofluid substantially enhances both skin friction and heat transfer rates compared to conventional hybrid nanofluids, due to the combined effects of ionic liquid properties and nanoparticle synergy. Quantitatively, increasing Cu fraction (from 0.001 to 0.01) raises the local Nusselt number by approximately 1.7% and skin-friction coefficient by approximately 2.7%, while delaying bifurcation onset by approximately 5.4% and lowering suction threshold by approximately 2.3%. The findings highlight the superior heat transfer capability of hybrid ionanofluids and establish their potential as next-generation working fluids in advanced thermal systems.

Keywords: MHD; Hybrid Ionanofluid; Heat Generation; Dual Solutions; Stability Analysis

How to cite this article
Datta A, Banerjee A, Mukherjee S. Magnetohydrodynamic Flow and Heat Transfer Enhancement with Al2O3-Cu Hybrid Ionanofluids over an Exponentially Stretching/Shrinking Permeable Sheet with Heat Generation and Slip Effect. Int. J. Nanosci. Nanotechnol., 2025;3: 123-136.
DOI: 10.22034/ijnn.2025.2066935.2685

1. Introduction

Technological advancements have highlighted the essential role of efficient heat transfer processes in various industrial sectors such as thermal power, chemical processing, manufacturing, and transportation. The development of high-performance heat transfer fluids is essential for enhancing operational efficiency and addressing increasing energy demands. Comprehensive reviews by Sidik et al. [1] and Huminic and Huminic [2] underscore the significant advancements made possible by the application of nanofluids. Maxwell [3] was the first to introduce the idea of improving the thermal conductivity of a conventional fluid through the suspension of micro-sized solid particles. Hamilton and Crosser [4] advanced predictive models for heterogeneous systems based on this foundation. Nonetheless, challenges including particle agglomeration and obstruction in flow channels have led researchers to investigate nanoscale suspensions. Choi and Eastman [5] introduced nanofluids, which consist of nanometer-sized particles dispersed in a base fluid, effectively reducing flow obstruction and significantly enhancing thermal properties. Hybrid nanofluids (HyNFs) [6-8] consist of two or more different types of nanoparticles dispersed in a base fluid, have been developed to improve thermal conductivity and convective heat transfer performance. HyNFs exhibit enhanced thermophysical characteristics compared to mono-nanofluids and conventional fluids. Consequently, their heat transfer mechanisms

[1] *Department of Mechanical Engineering, Institute of Engineering and Management, School of University of Engineering and Management (UEM), Kolkata, Saltlake Sector V, Kolkata – 700 091, India.*

[2] *Department of Mechanical Engineering, Dr. B. C. Roy Engineering College, Durgapur- 713206, India.*

[3] *Department of Mechanical Engineering, Gandhi Academy of Technology and Engineering, Brahmapur, Odisha,761008, India.*

E-mail: abanti.datta@gmail.com

and rheological behaviour have attracted significant research attention, reflecting the rapid advancement of thermal technologies.

Several studies have investigated on the convective heat and flow characteristics of nanofluids. Rohni et al. [9] examined the heat transfer rate and BL flow over a vertically oriented exponentially shrinking (SHR) sheet, identifying that a surface mass flux parameter S > 2.2667 is required to sustain a steady flow. Sathish et al. [10] conducted comparative analyses on the flow behaviour of non-Newtonian fluids on exponentially stretched sheets, highlighting distinct rheological properties. Merkin et al. [11] investigated on flow and heat transfer over a stretching (SCH) or shrinking (SHR) cylinder, demonstrating that unique solutions exist for SCH surfaces, whereas dual solutions emerge for SHR cases. Rehman et al. [12] explored the thermophysical characteristics of three-dimensional magnetohydrodynamic (MHD) stagnation-point flow of nanofluids over exponentially SCH surfaces. Further, Ghosh et al. [13] analyzed the flow and heat transfer behaviour of nanofluids over a SHR sheet incorporating heat and mass fluxes. In addition, Lund et al. [14] extended the analysis to address the existence of quadruple solutions in MHD nanofluid mixed convection flows over SHR/SCH vertical plates, supported by a detailed stability assessment. Variable viscosity and spontaneous convection on the BL flow were examined by Manjunatha et al. [15] for HyNFs. The authors reported that HyNFs enhance heat transfer more effectively than conventional nanofluids. Current research on mono and HyNF-based heat pipe technologies was reported by Bumataria et al. [16]. The thermal conductivity of HyNFs has recently been explored experimentally by Huminic et al. [17]. This was followed by research on HyNF flow, which revealed that the properties of HyNFs increase with concentration and temperature rise. Bhattacharyya [18] examined the HyNF flow induced by a SHR sheet in light of prior work on the boundary layer (BL) over non-linear surfaces. Vorticity cannot be limited in this fashion to the BL; hence similar solutions would not exist. The phenomenon of mixed convection flow was examined by Waini et al. [19] using a HyNF and a vertical surface that was rapidly stretching and shrinking. Furthermore, Dero et al. [20] conducted a stability investigation of Cu-$C_6H_9NaO_7$ and Ag-$C_6H_9NaO_7$ nanofluids using a single-phase model. The impact of viscosity on SCH sheets and SHR sheets was examined in this study. One solution exists when the SCH/SHR parameter λ is greater than a critical value λ_c; no solution exists when λ is less than λ_c. The critical point at which a solution becomes available is indicated by the subscript c. In a HyNF, Khashi'ie et al. [21] studied permeable power law deformable plates with perpendicular shear. The authors reported that λc is commonly observed in the SHR zone and is also known as a separation point. Zainal et al. [22] employed a bidirectional exponentially stretching or SHR sheet to evaluate the heat production or absorption in MHD flow for a HyNF. To show the stability of the solution, dual solutions were employed for the stability study. It was determined numerically that the positive eigenvalues of the upper branch were physically more stable than the lower branch's negative eigenvalues. As proven by Rao's research [23] the nanofluid stability is depends strongly on both working fluid performance and nanofluid preparation. Although the study of BL behavior on nonlinear surfaces has attracted growing attention, investigations specifically addressing exponential SCH or SHR surfaces remain relatively limited.

A new class of fluids, termed ionanofluids, has been introduced by Ribeiro et al. [24], where nanoparticles are suspended within ionic liquids rather than traditional solvents. Ionanofluids exhibit unique thermophysical properties [25-32]. While prior research has primarily focused on improving the thermal conductivity and viscosity of ionic liquids through the addition of nanoparticles like multi-walled carbon nanotubes, graphene, or Al_2O_3 nanoparticles, comprehensive studies on the convective transport behavior of ionanofluids, especially under BL configurations, are limited. The synergistic combination of low volatility, high thermal stability of ionic liquids, and enhanced transport properties of nanoparticles reveal ionanofluids as promising candidates for next-generation heat transfer applications, including solar thermal energy systems [26-29]. Reported enhancements of up to 30% in thermal conductivity and 10% in specific heat capacity further confirm their potential [31,32]. Asghar et al. [33] investigated slip effects on magnetized radiatively hybridized ferrofluid flows and highlighted the occurrence of dual solutions with stability implications. Recent studies [34-40] have further explored multiple solution behaviors and stability analyses in HyNF and ionanofluid flows under magnetic, radiative, porous, and slip conditions, providing valuable insights into boundary-layer dynamics. Additional investigations by Ramya et al. [41] and Peiravi and Ashabi [42] have examined the influence of magnetic fields on nanofluid flows over stretching sheets, contributing to a deeper understanding of MHD effects in boundary-layer phenomena.

From the above literature review, it is evident that while substantial progress has been made in understanding nanofluid and HyNF flows over nonlinear and exponentially deforming surfaces, and significant efforts have been devoted to the thermophysical characterization of ionanofluids, a critical research gap still persists. Specifically, the integration of hybrid ionanofluids that synergistically combine the improved heat transfer characteristics of ionic liquids and nanoparticles into BL MHD flow configurations remains relatively unexplored. Furthermore, the combined effects of magnetic fields, internal heat generation, and velocity and thermal slip conditions on the dual solution behavior and stability characteristics of hybrid ionanofluid flows over exponentially SHR surfaces have not been thoroughly investigated. The complex interplay between these processes may greatly impact the flow dynamics and heat transfer performance but has received limited attention in previous research. Therefore, a comprehensive numerical analysis addressing these linked effects is both timely and necessary to bring new insights into the potential of hybrid ionanofluids for advanced heat transfer applications.

To address the identified research gaps, a set of questions is formulated: How do hybrid ionanofluids affect local skin friction (Cf) and heat transfer on permeable exponentially SCH and SHR surfaces? What are the effects of magnetic field, suction, nanoparticle concentration, thermal slip, and heat generation on momentum and thermal BLs? Under what conditions do dual solutions appear, and which branch is physically stable? These questions can guide the numerical investigation and interpretation of the results. Based on these questions, the objective of our study is directed to numerically evaluate the steady BL flow and heat transfer behavior of a hybrid ionanofluid across a porous, exponentially diminishing surface in the incidence of a transverse magnetic field, internal heat production, and thermal slip effects. Al_2O_3-Cu nanoparticles are selected because of their complementing properties: Cu offers excellent thermal conductivity, while Al_2O_3 gives stability, low cost, and chemical resistance. Since water lowers viscosity and costs and ionic liquids improve thermal stability and nanoparticle dispersion, dispersing them in a water–$[C_2mim][CH_3SO_3]$ ionic liquid mixture improves heat transmission, stability, and energy performance. Overall, this hybrid nanofluid outperforms traditional systems in terms of heat transport efficiency. To achieve these objectives a hybrid suspension of copper (Cu) and alumina (Al_2O_3) nanoparticles distributed in a water–$[C_2mim]$ $[CH_3SO_3]$ ionic liquid mixture is regarded as the working fluid. To the best of the authors' knowledge, this constitutes the first effort to explore MHD BL flow and dual solution stability for hybrid ionanofluids across nonlinear exponentially shrinking surfaces. The governing equations are solved using MATLAB bvp4c, and a linear stability analysis is performed to locate the physically realizable solution. Parametric investigations are carried out to understand the impact of magnetic field strength, nanoparticle concentration, heat generation, suction, and slip parameters on the velocity, temperature, SFC and Nu. The findings provide critical insights into the local behavior of skin friction and heat transfer, which are significant for applications requiring enhanced convective heat transfer and controlled boundary layer development, including microchannel heat exchangers, electronic cooling systems, and solar thermal devices.

2. Mathematical modelling

Figure 1 illustrates the physical models. The velocity is defined as $u_w(x) = U_0 e^{x/L}$, where U_0 and L are constant velocity and characteristic surface length. The y direction is affected by the magnetic field variable $B(x) = B_0 e^{x/L}$, where B_0 is the constant. The volumetric heat generation (or absorption) is given by $Q(x) = Q_0 e^{x/L}$, where Q_0 is the constant for the heat sink or source. It ignores the impact of viscous dissipation. The wall temperature is considered as $T_w(x) = T_\infty + T_0 e^{x/L}$, where T_∞ and T_0 are the ambient temperature and the reference temperature. $T_0 > 0$ is known as secondary flow, and $T_0 < 0$ is leading flow. Also, the nanoparticles are assumed to be of the same size of 10^{-9} m. Due to the synthesis of stable hybrid ionanofluid, the aggregation of nanoparticles is disregarded. In the energy equation, the effect of heat radiation along the y axis on heat transfer is accounted for. Consequently, the continuity, the momentum, and the energy equations are (1) to (3), in that order. All the notations used in equations (1) to (3) are described in the Nomenclature.

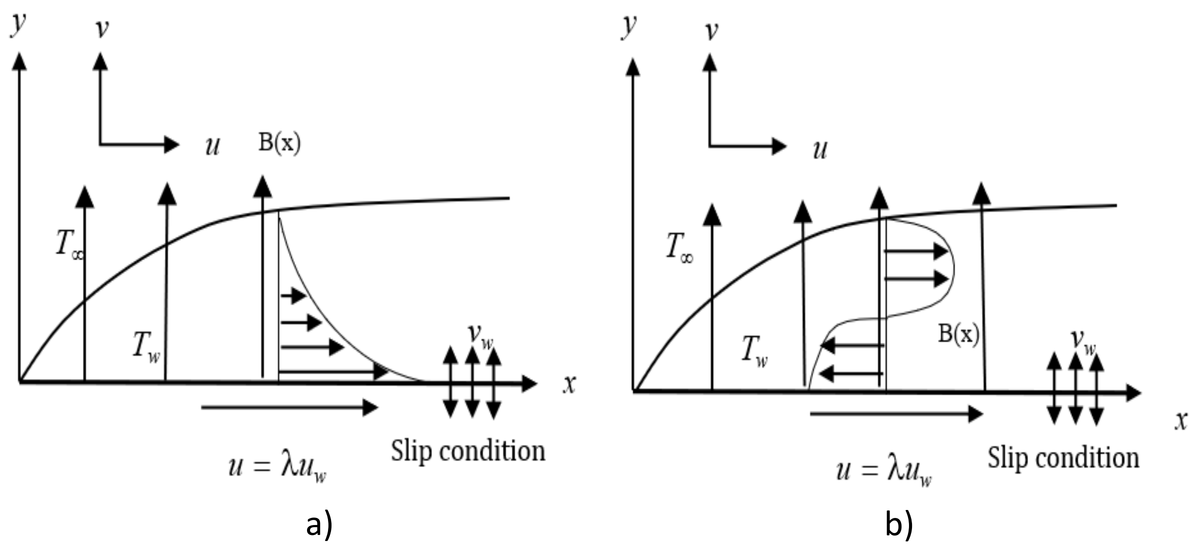

Figure 1. Physical models of (a) SCH (λ>0) and (b) SHR sheet λ<0.

Based on the BL assumptions, the governing equations ([43] and [44]), are written as follows:

$$\frac{\partial u}{\partial x}+\frac{\partial u}{\partial y}=0 \tag{1}$$

$$u\frac{\partial u}{\partial x}+v\frac{\partial u}{\partial y}=\frac{\mu_{inf}}{\rho_{inf}}\left[\frac{\partial^2 u}{\partial y^2}\right]-\frac{\sigma_{inf}}{\rho_{inf}}B^2(x)u \tag{2}$$

$$u\frac{\partial T}{\partial x}+v\frac{\partial T}{\partial y}=\frac{k_{inf}}{(\rho C_P)_{inf}}\left[\frac{\partial^2 T}{\partial y^2}\right]+\frac{Q(x)}{(\rho C_P)_{inf}}(T-T_\infty) \tag{3}$$

The boundary conditions (BCs) proposed by Ghosh and Mukhopadhyay [45], Mukhopadhyay and Andersson [46] are:

$$u=\lambda u_w(x)+A_1\frac{\mu_{inf}}{\rho_{inf}}\left(\frac{\partial u}{\partial y}\right), v=v_w(x), \quad T=T_w(x)+B_1\left(\frac{\partial T}{\partial y}\right) at\ y=0 \tag{4}$$

$$u\to 0, T\to T_\infty\ as\ y\to\infty$$

where A1 and B1 are the velocity and thermal slip factors, correspondingly. The previously mentioned governing equations are reduced into (Waini et al. [44], Eid and Nafe [48]):

$$\psi=e^{2x/L}\sqrt{2V_f Lc f(\eta)},$$

$$\theta(\eta)=\frac{T-T_\infty}{T_w-T_\infty},\ \eta=ye^{2x/L}\sqrt{\frac{c}{2V_f L}} \tag{5}$$

where ψ is the stream function and is defined as $u=\frac{\partial\psi}{\partial y}$ and $v=-\frac{\partial\psi}{\partial x}$ and equations (2) and (3) becomes into following equations:

$$\left(\frac{\mu_{inf}/\mu_f}{\rho_{inf}/\rho_f}\right)f'''+ff''-2f'^2-\left(\frac{\sigma_{inf}/\sigma_f}{\sigma_{inf}/\sigma_f}\right)M=0 \tag{6}$$

$$\frac{1}{Pr}\left(\frac{k_{inf}}{k_f}\right)\theta''+\frac{(\rho C_P)_{inf}}{(\rho C_P)_f}(f\theta'-f'\theta)+\beta\theta=0 \tag{7}$$

The transformed BCs are:

$$f(0)=S, f'(0)=\lambda+Af''(0), \theta(0)=1+B\theta'(0)$$

$$f'(\eta)\to 0, \theta'(\eta)\to 0\ as\ \eta\to\infty \tag{8}$$

Introducing the Prandtl number, $Pr=\frac{\mu_f(C_p)_f}{k_f}$, the heat generation parameter, $\beta=\frac{2Q_0 L}{c(\rho C_P)_f}$, the velocity slip parameter, $A=A_1(\mu_{inf}/\rho_{inf})e^{x/2L}\sqrt{c/2v_f L}$, the thermal slip parameter, $B=B_1 e^{x/2L}\sqrt{c/2v_f L}$, the wall mass transfer parameter, $S=-\frac{v_0}{\sqrt{v_f c/2L}}$- in which mass suction is $S<0\ (i.e., v_0>0)$ and mass injection is $S>0\ (i.e., v_0<0)$, the local SFC C_f and local Nu (Nu_x) are computed as in Hayat and Nadeem [48]:

$$C_f=\left(\frac{\mu_{inf}}{\rho_f}\right)\frac{1}{u_w^2}\left(\frac{\partial u}{\partial y}\right)_{y=0} \tag{9}$$

$$Nu_x=\left(\frac{k_{inf}}{k_f}\right)\frac{-2L}{(T_w-T_\infty)}\left(\frac{\partial T}{\partial y}\right)_{y=0} \tag{10}$$

The transformed equations finally become:

$$Re_x^{1/2}C_f=\left(\frac{\mu_{inf}}{\rho_f}\right)f''(0) \tag{11}$$

$$Re_x^{1/2}Nu_x=\left(\frac{k_{inf}}{k_f}\right)\theta'(0) \tag{12}$$

where $Re_x=2Lu_w/v_f$ is local Re. The equations are solved with the BCs equation (8). Since the boundary layer thickness, velocity gradients, and heat transfer rates evolve with *x* direction, using Re_x enables accurate representation of the local variations in skin friction and heat transfer.

3. Flow stability

The flow stability study is carried out because dual solutions can be computed. To achieve this, time-dependent terms are introduced into equations (2) and (3), making them:

$$u\frac{\partial u}{\partial x}+v\frac{\partial u}{\partial y}+\frac{\partial u}{\partial t}=\left(\frac{\mu_{inf}}{\rho_{inf}}\right)\frac{\partial^2 u}{\partial y^2}-\left(\frac{\sigma_{inf}}{\rho_{inf}}\right)B^2(x)u \tag{13}$$

$$u\frac{\partial T}{\partial x}+v\frac{\partial T}{\partial y}+\frac{\partial T}{\partial t}=\left(\frac{k_{inf}}{(\rho C_P)_{inf}}\right)\frac{\partial^2 T}{\partial y^2}+\frac{Q}{(\rho C_P)_{inf}}(T-T_\infty) \tag{14}$$

where t is time. Based on the previous studies (Waini et al. [44], Merkin [49], Weidman et al. [50] and Yan et al. [51]) variable transformation is as follows:

$$\eta=ye^{x/2L}\sqrt{\frac{c}{2V_f L}}, \psi=f(\eta,\tau)\sqrt{2cV_f L},$$

$$\theta(\eta,\tau)=\frac{T-T_\infty}{T_w-T_\infty}, \tau=e^{x/L}\frac{c}{2L} \tag{15}$$

Using the transformation, the equations become:

$$\left(\frac{\mu_{inf}/\mu_f}{\rho_{inf}/\rho_f}\right)\frac{\partial^3 f}{\partial\eta^3}+f\frac{\partial^2 f}{\partial\eta^2}-2\left(\frac{\partial f}{\partial\eta}\right)^2 -\frac{\partial^2 f}{\partial\eta\partial\tau}-\left(\frac{\sigma_{inf}/\sigma_f}{\sigma_{inf}/\sigma_f}\right)M=0 \quad (16)$$

$$\frac{1}{Pr}\left(\frac{k_{inf}}{k_f}\right)\frac{\partial^2\theta}{\partial\eta^2}+\frac{(\rho C_P)_{inf}}{(\rho C_P)_f}\left(f\frac{\partial\theta}{\partial\eta}-\frac{\partial f}{\partial\eta}\theta-\frac{\partial\theta}{\partial\tau}\right)+\beta\theta=0 \quad (17)$$

Restricted conditions:

$$f(0,\tau)=S,\ \frac{\partial f}{\partial\eta}(0,\tau)=\lambda+A\frac{\partial^2 f}{\partial\eta^2}(0,\tau),$$

$$\theta(0)=1+B\frac{\partial\theta}{\partial\eta}(0,\tau)$$

$$\frac{\partial f}{\partial\eta}(\eta,\tau)\rightarrow 0,\theta'(\eta,\tau)\rightarrow 0\ as\eta\rightarrow\infty \quad (18)$$

The following perturbation is introduced to examine the stability of the similarity solutions, $f(\eta)=f_0(\eta)$ and $\theta(\eta)=\theta_0(\eta)$:

$$f(\eta,\tau)=f_0(\eta)+e^{-\gamma\tau}F(\eta)$$

$$\theta(\eta,\tau)=\theta_0(\eta)+e^{-\gamma\tau}G(\eta) \quad (19)$$

where γ is an unknown eigenvalue and $F(\eta)$ and $G(\eta)$ are small compared to $f_0(\eta)$ and $\theta_0(\eta)$, respectively (Waini et al. [44], Weidman et al. [50], and Yan et al. [51]). Equations (16) to (18) can be linearized by substituting equation (19) and setting t = 0 to examine the initial growth or decay of disturbances in equation (19):

$$\left(\frac{\mu_{inf}/\mu_f}{\rho_{inf}/\rho_f}\right)F'''+Ff_0''+F''f_0-4F'f_0' +\gamma F'+\left(\frac{\sigma_{inf}/\sigma_f}{\sigma_{inf}/\sigma_f}\right)M=0 \quad (20)$$

$$\frac{1}{Pr}\left(\frac{k_{inf}}{k_f}\right)G''+\frac{(\rho C_P)_{inf}}{(\rho C_P)_f}\left(F\theta_0'-G'f_0-Gf_0'+\gamma G\right)+\beta G=0 \quad (21)$$

In accordance with the linearized requirements:

$$F'(\infty)\rightarrow 0,G(\infty)\rightarrow 0" \quad (22)$$

Because the majority of the linearized conditions in equation (22) have values that are equivalent to zero, it is necessary for $F'(\infty)\rightarrow 0$ to be relaxed and substituted with $F''(0)=1$ in order to provide a series of eigenvalues that are realisable. Consequently, the bvp4c solver is applied to determine the unknown eigenvalues, which serve as an indicator for determining the stability of the flow. When the eigenvalue falls below 0, the flow is considered unstable, and when it rises over 0, it is considered stable.

It should be noted that the parameter values used in this study were selected to reflect realistic conditions in engineering applications. The magnetic parameter *M* was varied to represent moderate electromagnetic effects commonly considered in MHD studies. Suction parameter *S* was chosen to explore its effect on BL control, while nanoparticle volume fractions ϕ_{p1} and ϕ_{p2} were selected based on typical concentrations that enhance thermal conductivity without causing excessive viscosity. Thermal slip *B* and heat generation and *β* values were adopted from prior studies to investigate their impact on heat transfer and flow characteristics. These selections ensure that the results are both physically meaningful and relevant to various thermal applications.

4. Thermophysical properties of the hybrid ionanofluid

In this paper, a mixture of water–[C_2mim][CH_3SO_3] ionic liquid is taken as the base fluid which is hybridized with alumina and copper nanoparticles. The volume fraction of nanoparticles is varied as 0.001%, 0.005% and 0.01%. The physical properties of all nanoparticles, water and ionic liquids are given in Table 1.

The mass balance is used to determine the hybrid ionanofluid density, which is similar to that of the single nanofluid [54]:

$$\rho_{inf}=\phi_{p1}\rho_{p1}+\phi_{p2}\rho_{p2}+(1-\phi)\rho_{bf}$$

Table 1. Thermophysical properties of nanoparticles, water and ionic liquid.

Material	Density (kg/m^3)	Specific heat (J/kg.K)	Thermal conductivity (W/m.K)	Electrical conductivity (S/m)	References
Water	998.2	4182	0.597	0.05	Datta and Halder [46]
Water–IL mixture (0.25:0.75)	1237	1771.9	0.201	0.8064	Chereches and Minea [52]
Al_2O_3	3880	773	36	35 × 10^6	Datta and Halder [46]
Cu	8940	385	390	59.6 × 10^6	Datta et al. [53]

$$\phi = \phi_{p1} + \phi_{p2} \tag{23}$$

The density of the base fluid (ionic liquid) is specified by ρ_{bf}, and ϕ is the total volume fraction (VF) of two different nanoparticles suspended in the ionic liquid, where ϕ_{p1} refers to the Al_2O_3 nanoparticles and ϕ_{p2} refers to the Cu nanoparticles. The specific heat of the hybrid ionanofluid is determined using an energy balance identical to that of a single nanofluid:

$$C_{Pinf} = \phi_{p1}\rho_{p1}C_{Pp1} + \phi_{p2}\rho_{p2}C_{Pp2} + (1-\phi)C_{Pbf}\rho_{bf}. \tag{24}$$

Brinkman [55] expanded the Einstein equation to a nanoparticle VF of up to 4%:

$$\mu_{inf} = \frac{1}{(1-\varphi)^{2.5}}\mu_{bf} \tag{25}$$

Several researchers estimated the heat conductivity of single nanofluid using the Maxwell model [3]. To determine the hybrid ionanofluid's thermal conductivity, the thermophysical properties of the solid nanoparticles and the ionic liquid are substituted into the equation. The revised Maxwell model is:

$$k_{inf} = k_{bf}\left[\frac{\dfrac{\phi_{p1}k_{p1}+\phi_{p2}k_{p2}}{\phi} + 2k_{bf} + 2(\phi_{p1}k_{p1}+\phi_{p2}k_{p2}) - 2k_{bf}}{\dfrac{\phi_{p1}k_{p1}+\phi_{p2}k_{p2}}{\phi} + 2\phi k_{bf} - (\phi_{p1}k_{p1}+\phi_{p2}k_{p2}) - \phi k_{bf}}\right] \tag{26}$$

The Hamilton and Crosser model [4] is used to calculate the electrical conductivity of the material. This model is then modified based on the Maxwell model [3] and the revised equation is:

$$\sigma_{inf} = \sigma_{bf}\left[\frac{\dfrac{\phi_{p1}\sigma_{p1}+\phi_{p2}\sigma_{p2}}{\phi} + 2\sigma_{bf} + 2(\phi_{p1}\sigma_{p1}+\phi_{p2}\sigma_{p2}) - 2\sigma_{bf}}{\dfrac{\phi_{p1}\sigma_{p1}+\phi_{p2}\sigma_{p2}}{\phi} + 2\phi\sigma_{bf} - (\phi_{p1}\sigma_{p1}+\phi_{p2}\sigma_{p2}) - \phi\sigma_{bf}}\right] \tag{27}$$

5. Numerical Analysis

For the BL flow and heat enhancement, the governing nonlinear ODEs are solved using the bvp4c (boundary value problem solver) in MATLAB. The bvp4c solver provides the numerical solution using the three-stage Lobatto IIIa method proposed by Kierzenka and Shampine [56]. This method has a predetermined level of accuracy as it starts with guess at the initial mesh points and then gradually increases the step size. The tolerance level is set to 10^{-10} in the present computations. In comparison to the shooting method and the Keller box method, the bvp4c solver produces satisfactory solutions, according to Waini et al. [44]. In this analysis, both $(\lambda > 0)$ and $(\lambda < 0)$ are considered. Throughout the analysis, Al_2O_3 nanoparticles VF is assumed as $\phi_{p2} = 0.01$. Other constraints, for example velocity slip A and thermal slip B, magnetic parameter M, Cu nanoparticles VF ϕ_{p2}, heat generation β, and suction S are altered to analyze the effect on BL flow and heat transfer. The structure of the process is shown in the flowchart (Figure 2).

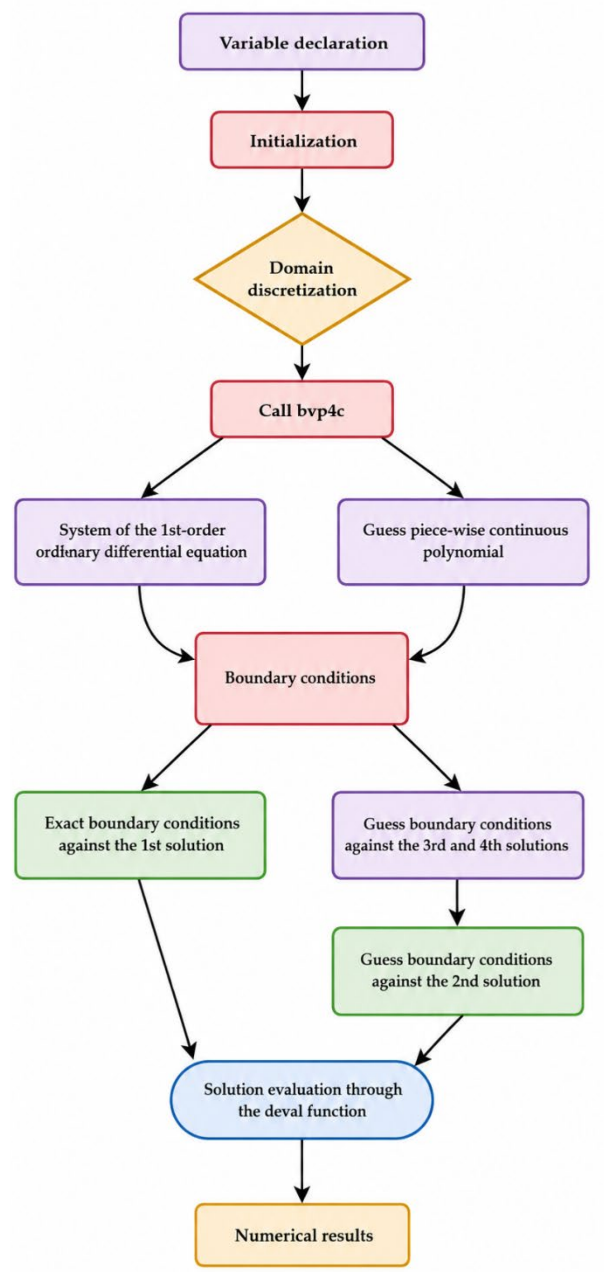

Figure 2. Flowchart of the numerical solution procedure.

6. Validation

Prior to the detailed analysis of the Cu–Al_2O_3/water–[C_2mim] [CH_3SO_3] hybrid ionanofluid, a baseline simulation was performed using pure water to validate the computational model. The numerical results were benchmarked against the established data reported by Waini et al. [44], Ghosh and Mukhopadhyay [45], Hafidzuddin et al. [57], and Ishak [58]. For a viscous fluid and a SHR surface condition (λ = −1), the SFC and the associated heat transfer quantity are computed and compared, as summarized in Table 2 (with S = 3 and Pr = 0.7). Both the primary and secondary solution branches show excellent agreement with the referenced studies, demonstrating the robustness of the numerical method. This validation confirms that the bvp4c solver accurately captures the physical behaviour of the BL flow.

Furthermore, the findings underscore that the intensity of suction employed in the model plays a critical role in suppressing BL separation, thereby facilitating the gradual transport of nanoparticles within the flow domain.

Table 3 presents the numerical values of $-\theta'(0)$ for various values of Prandtl number and magnetic parameter, which are compared with the results from earlier studies [44, 58-60]. This table demonstrates numerical results are in close agreement with previously reported results. With an increase in the Prandtl number the temperature BL thickness decreases and heat transfer efficiency increases. Consequently, the heat transfer efficiency is improved.

7. Result and discussion

MHD flow and heat transfer with hybrid ionanofluid and standard HyNFs are studied numerically to find the optimum nanofluids for heat transfer augmentation. Figure 3(a) and 3(b) illustrate the variation of $Re_x^{1/2}C_f$ and $Re_x^{1/2}Nu_x$ for hybrid ionanofluid and standard hybrid nanofluid. In comparison with hybrid ionanofluid and HyNFs, the hybrid ionanofluid has a higher value of $Re_x^{1/2}C_f$, as shown in Figure 3(a). This occurs because the hybrid ionanofluid possesses greater viscosity and a thinner velocity boundary layer than the standard hybrid nanofluid, resulting in increased wall shear stress and, consequently, a larger skin friction coefficient. Furthermore, the ionic nature of the base fluid enhances momentum transfer near the wall due to stronger electrostatic interactions, which also contributes to the rise in $Re_x^{1/2}C_f$.

In Figure 3(b), the region $(\lambda < -1)$ demonstrated that hybrid ionanofluid has a higher value of $Re_x^{1/2}Nu_x$ compared to standard hybrid nanofluid. This enhancement can be attributed to the synergistic effect of nanoparticles and the ionic fluid, whose distinct thermophysical properties (e.g., higher thermal conductivity, altered specific heat, and modified Prandtl number) significantly influence the local temperature gradient on the permeable exponentially SHR surface in the region. The thermal BL thickness in Cu-Al_2O_3 hybrid ionanofluid is less than that of Cu-Al_2O_3/water nanofluid, indicating efficient heat transfer augmentation with hybrid ionanofluids.

In comparison between hybrid ionanofluid and standard HyNFs, the hybrid ionanofluid has a higher value of $Re_x^{1/2}C_f$, as shown in Figure 3(a). Because of greater viscosity and thinner BL of the hybrid ionanofluid than HyNFs, the shear stress is increased which caused the higher value of $Re_x^{1/2}C_f$. In the region (λ<-1), Figure 3(b) demonstrates that hybrid ionanofluid has higher value of $Re_x^{1/2}Nu_x$ compared to standard HyNFs. This is due to the different thermophysical characteristics of ionic fluid and nanoparticles, which affect the temperature gradient and heat transfer rate on the permeable SHR surface in the region (λ<-1). Compared to Cu-Al_2O_3/water nanofluid, the hybrid ionanofluid has a lower thermal BL thickness. Thus, compared to Cu-Al_2O_3/water HyNFs, hybrid ionanofluid has a higher heat transfer augmentation.

Figures 4(a) and 4(b) illustrate the influence of M (0.2, 0.4, 0.6) in the variations of $Re_x^{1/2}C_f$ and $Re_x^{1/2}Nu_x$ with the

Table 2. Values of f''(0) and −θ'(0) for a viscous fluid (ϕ_{p1}=ϕ_{p2}=0), with Pr=0.7, S=3, and A=B=β=M=0, for λ = −1.

	$f''(0)$		$-\theta'(0)$	
	First solution	Second solution	First solution	Second solution
Waini et al. [42]	2.390814	-0.972247	1.771237	0.848316
Ghosh and Mukhopadhyay [43]	2.39082	-0.97223	1.77124	0.84832
Hafidzuddin et al. [55]	2.3908	-0.9722	1.7712	0.8483
Ishak [56]	2.390814	-0.972247	1.771237	0.848316
Present numerical value	2.390813487	-0.972127692	1.771237308	0.847731569

Table 3. Comparison of the numerical values -θ'(0) for (λ = -1), (ϕ_{p1} = ϕ_{p2} = 0).

$-\theta'(0)$						
Magnetic parameter(M)	Prandtl number (Pr)	Bidin and Nazar [60]	Magyari and Keller [59]	Ishak [8]	Waini et al. [44]	Present numerical value
0	0.5		0.594338		0.594339	0.596687591
0	1	0.9548	0.954782	0.9548	0.954783	0.954810645
0	2	1.4714		1.4715	1.47146	1.471454036
0	3	1.8691	1.869075	1.8691	1.869074	1.869068799
0	5		2.500135	2.5001	2.500132	2.500128788
0	10		3.660379	3.6604	3.660372	3.660369290
1	25	0.5315				0.535401194
1	1			0.8611	0.861094	0.873201623
1	0			0.5312	0.531158	0.535301196

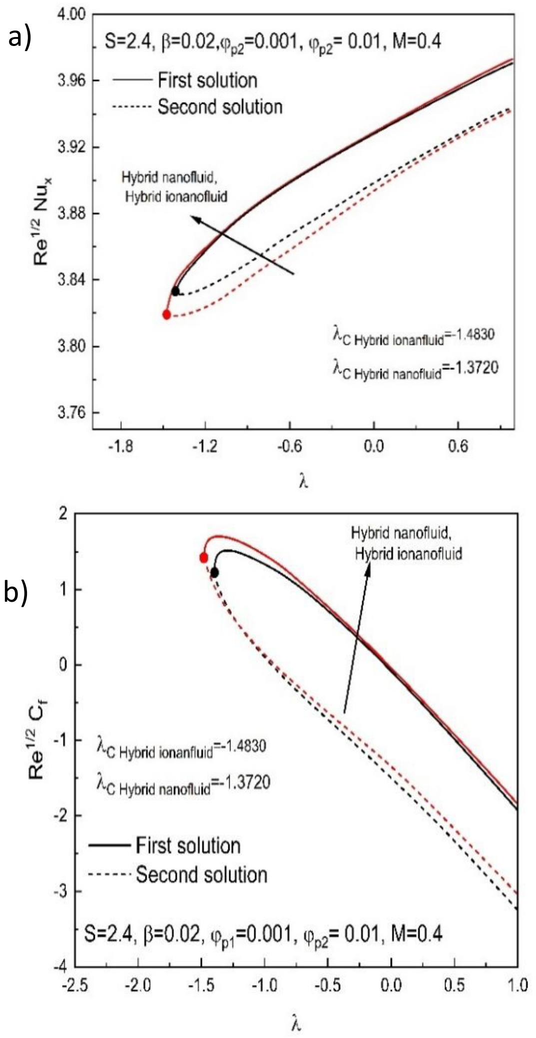

Figure 3. (a) Local SFC with Hybrid ionanofluid and Standard HyNFs and (b) local Nu with Hybrid ionanofluid and Standard HyNFs.

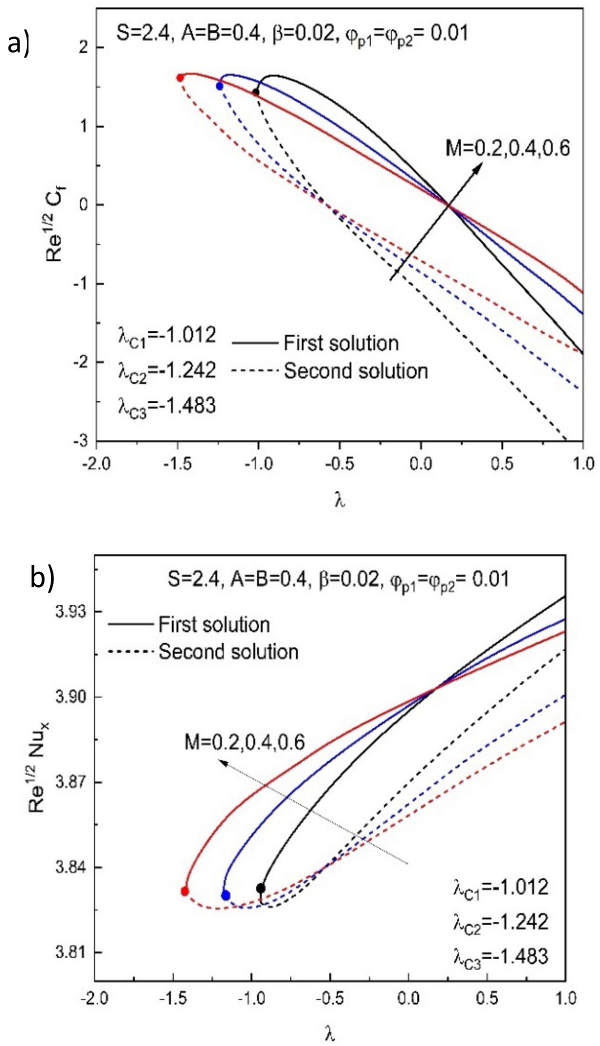

Figure 4. (a) Local SFC with λ on various values of M for hybrid ionanofluid (b) Local Nu versus λ on various values of M for Hybrid ionanofluid.

SCH / SHR parameter λ when S = 2.4, A = B = 0.4, β = 0.02, and $\phi_{p1} = \phi_{p2} = 0.01$. In Figure 4(a), the upper and lower branches describe the increase in $Re_x^{1/2} C_f$ on the exponential SCH surface when M is increased. This trend is primarily due to the stronger Lorentz force generated by the interaction of the magnetic field with the induced electric currents in the electrically conducting ionanofluid, which acts as a resistive drag opposing the fluid motion. The result is an enhancement of shear stress near the wall and a reduction in the thickness of the momentum BL, a phenomenon commonly observed in MHD flows. Moreover, the magnitude of $Re_x^{1/2} C_f$ is directly related to the magnetic damping effect, which modifies the velocity gradient near the surface.

Figure 4(b) illustrates a similar pattern of heat transfer, where the value of $Re_x^{1/2} Nu_x$ increases with M. The Lorentz force indirectly contributes to heat transfer augmentation by suppressing velocity fluctuations while intensifying the temperature gradient at the wall. This results in stronger convective heat flux and a thinner thermal BL enhancing the local rate of heat transfer. From a mathematical standpoint, the Nusselt number scales with the wall temperature gradient as $Nu_x \propto -\left(\frac{\partial T}{\partial y}\right)_{y=0}$ and the M increases this gradient by constraining fluid motion and forcing more efficient thermal conduction near the wall.

Figures 4(a) and 4(b) also demonstrate that as M increases, the surface region affected by MHD effect broadens. Moreover, as the parameter (λ<0) increases, the BL detachment is delayed, while the critical value λ_c decreases. This behavior is attributed to the combined effect of magnetic damping and wall-suction effect, $S>0$, both of which stabilize the flow and control the development of velocity and thermal BLs. Thus, the MHD mechanism not only augments friction and heat transfer but also provides a stabilizing influence that mitigates boundary layer separation on SHR surfaces.

Figure 5(a) shows the growth of local SFC on the permeable SHR surface with increasing VF of copper nanoparticles ϕ_{p2} when S = 2.4, A = B = 0.4, β = 0.02, and M=0.4. As the volume fraction of copper nanoparticles (ϕ_{p2}) increases, the effective viscosity and density of the hybrid ionanofluid rise. Due to this, the momentum diffusion enhances near the surface and causes a reduction in the thickness of the momentum BL. This results in an increment of $Re_x^{1/2} C_f$. As a result, shear

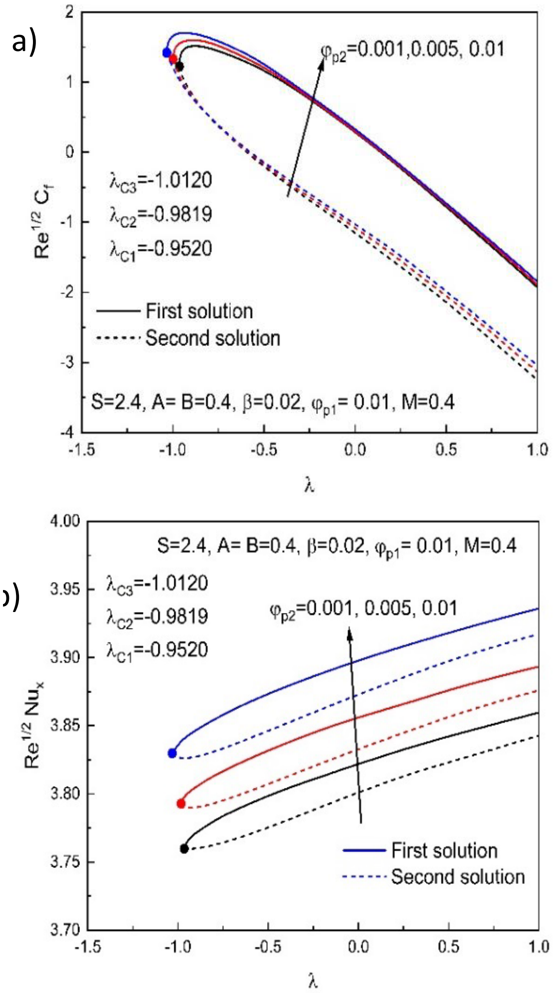

Figure 5. (a) Local Nusselt number versus λ on various volume fractions of Cu for Hybrid (b) Local Nu versus λ on various volume fractions of Cu for hybrid ionanofluid.

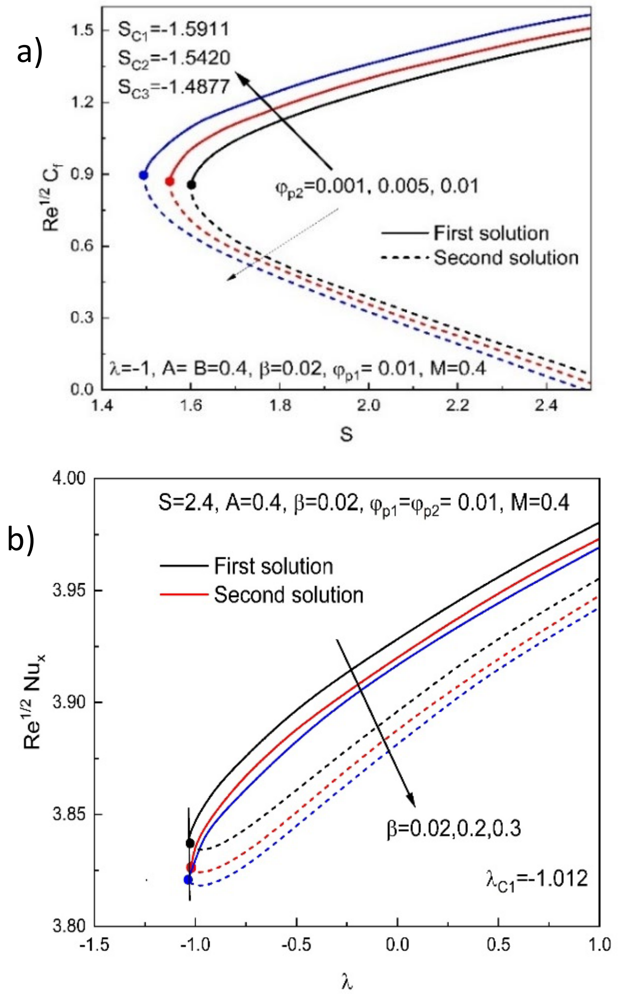

Figure 6. (a) Local SFC with S on various volume concertation of Cu for Hybrid ionanofluid and (b) Local Nu versus S on various volume concertation of Cu for Hybrid ionanofluid.

stress has a stronger impact on the permeable shrinking surface. Physically, the nanoparticles intensify micro-scale interactions within the fluid, thereby amplifying the viscous effects and modifying the velocity gradients in the near-wall region. Quantitatively, at λ = -1, $\mathrm{Re}_x^{1/2}\mathrm{Nu}_x$ increases from 3.8844 ($\phi_{p2} = 0.001$) to 3.9494 ($\phi_{p2} = 0.01$), a 1.67% gain, while $\mathrm{Re}_x^{1/2}\mathrm{C}_f$ rises from 4.0884 to 4.1990, a 2.70% increase. These values confirm the enhancing role of Cu addition on local transport properties.

Figure 5(b) shows the numerical solution for the variation of local Nusselt number with the SCH or SHR parameter λ for S = 2.4, A = B = 0.4, β = 0.02 and M = 0.4, whereas ϕ_{p2} increases from 0.001 to 0.01. When the ϕ_{p2} value grows, $Re_x^{1/2}Nu_x$ drops in the region $(-1 < \lambda < 0)$. This occurs due to the weaker shrinking strength, which reduces the convective transport efficiency. However, on an exponentially SHR surface, the dominant effect of thermal conductivity enhancement in the hybrid ionanofluid promotes the heat flux in the region $(\lambda < -1)$, while the heat flux falls in region $(-1 < \lambda < 0)$. In the region $(\lambda < -1)$, when ϕ_{p2} rises, the thermal boundary layer thickness decreases, leading to enhanced heat transfer through the exponentially contracting surface.

Figures 5(a) and 5(b) further reveal the existence of dual solutions for ϕ_{p2} (= 0.001, 0.005, 0.01) at λ_{C1} = -0.9520, λ_{C2} = -0.9819, and λ_{C3} = -1.0120, indicating the bifurcation points of the BL in the region (λ<0). The presence of copper VF postpones the separation of the BL by increasing fluid inertia and providing additional resistance against detachment. This stabilizing effect becomes stronger as the volume fraction increases, thereby extending the solution domain before flow reversal or boundary layer breakdown occurs.

Figures 6(a) and 6(b) illustrate the variation of the same parameters against S when λ = -1 and A = B = 0.4. An increase in copper VF parameter ϕ_{p2} is associated with increment of SFC $\mathrm{Re}_x^{1/2}\mathrm{C}_f$ at (λ<0) for the first solution but a decrease for the second solution, suggesting a shift in the stability characteristics of the flow. When λ<0, it is observed that there is a pattern transition of the SFC $\mathrm{Re}_x^{1/2}\mathrm{C}_f$ for the first solution as the copper VF parameter ϕ_{p2} increase. Additionally, the local Nu $\mathrm{Re}_x^{1/2}\mathrm{Nu}_x$ rises when the copper VF ϕ_{p2} increases for both solutions. When the SCH/SHR parameter λ decreases for both solutions, it is observed that $\mathrm{Re}_x^{1/2}\mathrm{C}_f$ and $\mathrm{Re}_x^{1/2}\mathrm{Nu}_x$ increase and decrease, respectively. Dual solutions appear to exist for ϕ_{p2} (= 0.001,

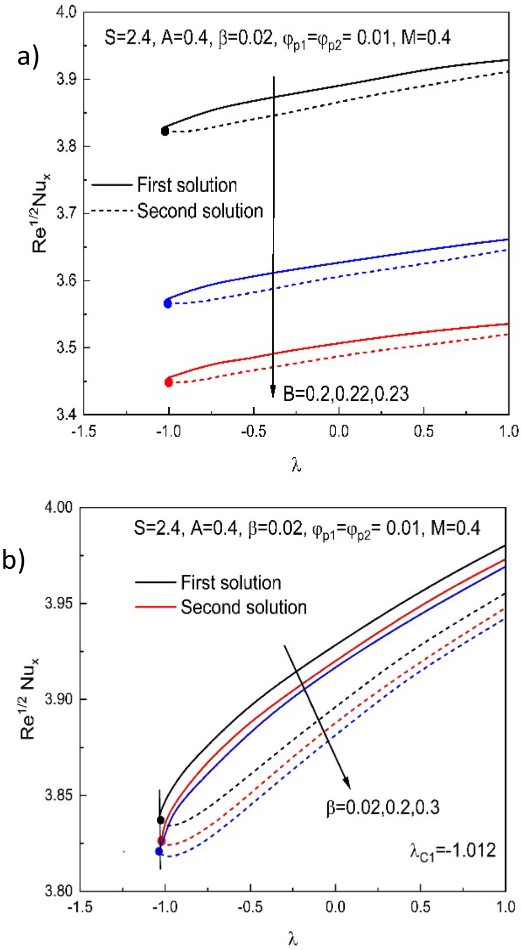

Figure 7. (a) Local SFC against λ on different values of thermal slip B and (b) Local Nu versus λ on different values of heat generation.

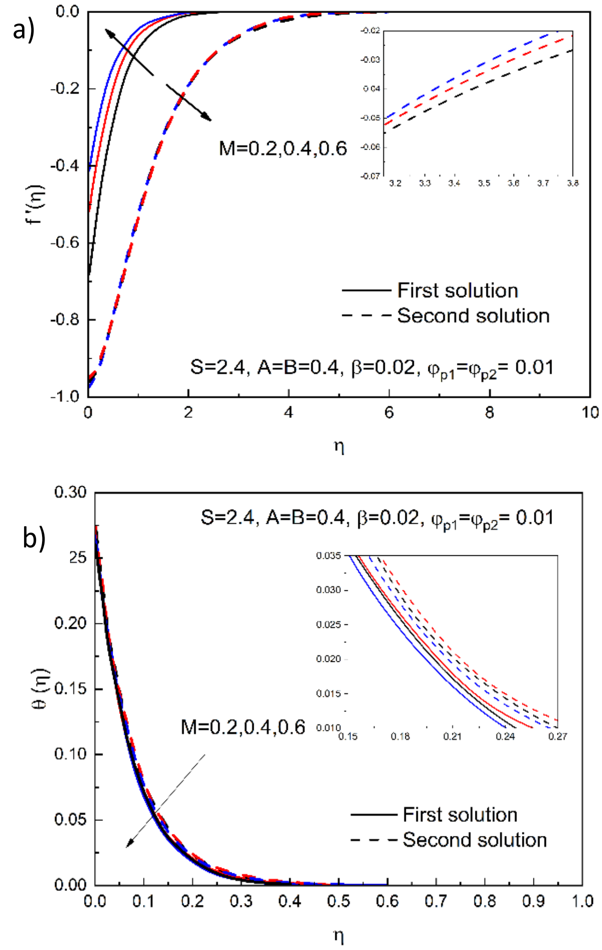

Figure 8. (a) Velocity profile on different values of M and (b) Temperature profile on different values of M.

0.005, and 0.01) in Figures 5(a) and (b) at S_{C1} = 1.5911, S_{C2} = 1.5420, and S_{C3} = 1.4877, indicating that specific suction levels are necessary to maintain flow stability and ensure dual solutions for the shrinking surface. Moreover, with higher ϕ_{p2} and S, the $Re_x^{1/2}C_f$ increases for the first solution but decreases for the second solution, whereas the $Re_x^{1/2}Nu_x$ steadily increases for both. This trend is consistent with the quantitative decrease in S_C from 2.0775 ($\phi_{p2} = 0.001$) to 2.0290 ($\phi_{p2} = 0.01$), i.e., approximately a 2.3% reduction, which indicates that Cu loading lowers the suction threshold for dual solutions.

Figures 7(a) and 7(b) depict the relationship between $\mathrm{Re}_x^{1/2}\mathrm{Nu}_x$ and the SCH or SHR parameter for different values of B = (0.2, 0.22, 0.23) and β = (0.02, 0.2, 0.3) when S = 2.4, ϕ_{p2} = 0.01, and A = 0.2. Although variations in B and β do not significantly alter the critical value λ_C (≈ - 1.4419), their influence on heat transfer characteristics is notable. An increase in thermal slip weakens the coupling between the wall and fluid temperature, reducing the ability of the fluid to absorb heat directly from the surface, thereby lowering $\mathrm{Re}_x^{1/2}\mathrm{Nu}_x$. Similarly, higher heat generation introduces additional thermal energy within the BL, diminishing the local temperature gradient and, hence, the Nu. Despite this reduction, both parameters lead to an upward trend in $\mathrm{Re}_x^{1/2}\mathrm{Nu}_x$ with increasing λ, suggesting that stronger stretching enhances convective transport even under slip and volumetric heating effects. Specifically, for ϕ_{p2} = 0.01, increasing slip (A = 0.2 to 0.6) shifts λ_c from −1.4419 to −2.0362, a $\sim 41\%$ extension of the shrinking domain before bifurcation.

In Figures 2-7, it can be noticed that the plotlines of the SFC and the local Nu with the SCH or SHR, as well as the suction parameters move towards the left side of the field, either up or down, to reach the critical point. There is just one solution to the problem at the critical point λ_c. Using the Tiwari and Das model [61], few parameters are used to explain the flow and heat transmission of MHD HyNFs on the permeable SHR surface. This particular scenario demonstrates the irreconcilability of the mathematical model in this region. There is no numerical solution for the region $\lambda < \lambda_c$. The SHR instance invalidates the Tiwari and Das model [61], which was created and applied using BL approximation theory, as shown by the separation of the boundary condition from the rapidly uneven surface. For a specific range of λ values, the second solution is only applicable. Reason for this behaviour is that the certain value of λ cannot monitor the precise solution due to limited relative error tolerance.

Increases in M (= 0.2, 0.4, 0.6) and S (= 2.2, 2.3, 2.4) cause the velocity profile f′(η) for the first solution to increase and the second solution to decrease, while both solutions of θ′(η) decrease, as depicted in Figures 8(a, b) and 9(a, b). For the 1st solution, a high degree of velocity slip is required to increase the flow velocity and vice versa because the presence of velocity slip at the shrinking surface boundary reduces the flow resistance, allowing more flow to slip through the surface and increasing the flow velocity.

For the copper volume concentration parameter ϕ_{p2} = (0.001, 0.005, 0.01), the increase in value enhances the f′(η) and θ′(η) profiles for both solutions, as shown in Figures 10(a) and 10(b). However, the f′(η) for the

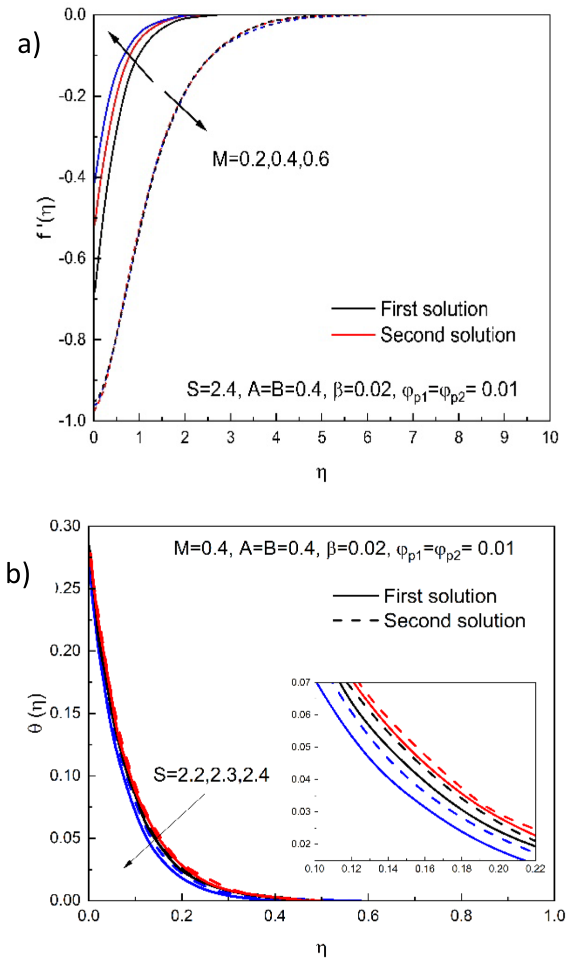

Figure 9. (a) Velocity profile for different values of suction, S, and (b) Temperature profile on different values of suction, S.

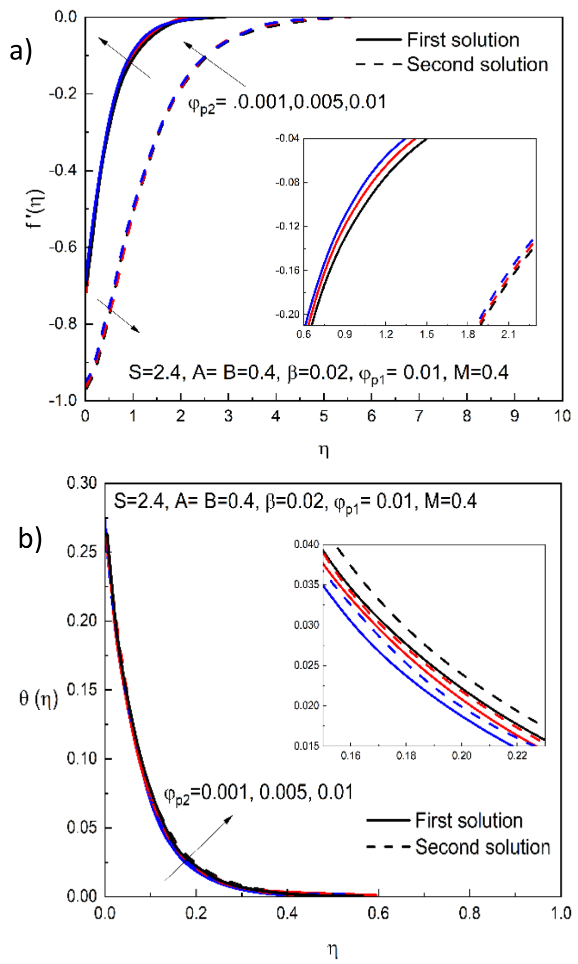

Figure 10. (a) Velocity profile for different copper volume fractions and (b) Temperature profile on different volumetric concentration of Cu.

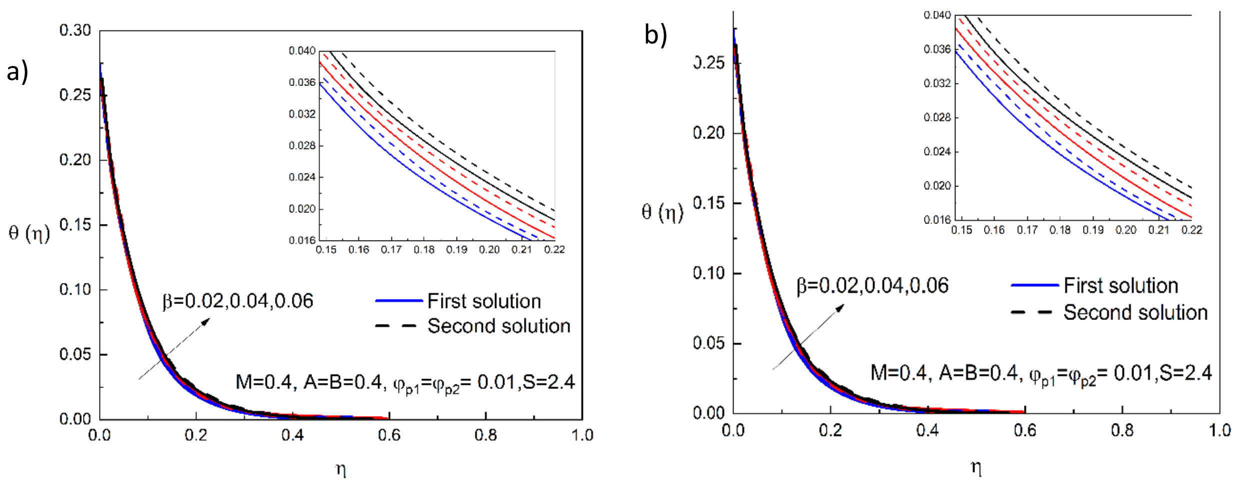

Figure 11. (a) Temperature profile on different values of thermal slip parameter, B and (b) temperature profile on different values of heat generation parameter, β.

second solution exhibits different behavior within a certain range. Assuming different values for the missing initial conditions under the same conditions yields two solutions for boundary value problems that have dual solutions. Knowing which option is physically acceptable is essential. The first approach is more common in practice and is physically more stable than the second. Only the viability of the first solution is covered in this work. The flow is unstable, as indicated by the negative eigenvalues against the controlling parameters in the second solution.

Figures 11(a, b) depict the effects of of the parameters B and β (the parameters B=0.2, 0.4, and 0.6 and β=0.02, 0.04, and 0.06 on the temperature profile). Since these parameters do not affect $f'(\eta)$, only the temperature profile $\theta'(\eta)$ is considered in this study. When B decreases and β increases, $\theta'(\eta)$ is observed to rise. To achieve the desired heat transfer performance, it is necessary to control the thermal slip and heat generation parameters in the correct proportions, as each parameter has a distinct effect that could be offset by the other.

8. Conclusions

We have studied steady MHD BL flow and heat transfer of a $Cu–Al_2O_3/[C_2mim][CH_3SO_3]$ hybrid ionanofluid over an exponentially SCH/SHR permeable sheet, including velocity and thermal slip effects and internal heat generation. The governing equations were reduced using similarity transformations and then solved numerically using MATLAB bvp4c solver. A linear stability analysis was performed to determine the physically realizable solution branch.

The main conclusions are as follows:

I. Dual similarity solutions arise for the SHR surface when suction is sufficiently strong. The upper branch is the only one that is stable and physically significant, according to linear stability assessment.
II. Increasing the magnetic parameter M elevates both the SFC and the Nu, due to stronger Lorentz forces that retard the flow and steepen the temperature gradient at the wall.
III. A higher VF of Cu nanoparticles increases the fluid viscosity and thermal conductivity, which in turn raises the wall shear stress and enhances heat transfer. Quantitatively, Cu addition (from 0.001 to 0.01) increases $_{Nu}$ by approximately 1.7%, C_f by approximately 2.7%, shifts λ_c by approximately 5.4%, and reduces Sc by approximately 2.3%.
IV. Larger thermal slip or stronger internal heat generation tends to reduce the heat transfer rate (lower Nu) by weakening the wall temperature gradient.
V. For all conditions examined, the ionic-liquid-based HyNF produces higher C_f and Nu than the corresponding $Cu–Al_2O_3$/water nanofluid, demonstrating its superior heat transfer capability.

The enhanced heat transfer performance of hybrid ionanofluids highlights their potential in real-world thermal management applications, like electronic cooling, solar thermal collectors, energy storage systems, and advanced heat exchangers. In particular, the consideration of exponentially SHR/SCR permeable surfaces provides insights into flow and heat transfer behaviors relevant to industrial processes such as polymer extrusion, glass and metal manufacturing, and coating technologies, where surface deformation and suction/injection significantly influence product quality and thermal performance. Beyond these applications, the present findings establish a foundation for future research directions. The numerical framework presented here can be extended to experimental validation, as well as to more complex regimes such as turbulent and transient flows or alternative ionic liquid-based suspensions. Moreover, further studies on scale-up effects, long-term stability, and compatibility with industrial processes will be essential to ensure that hybrid ionanofluids can transition from theoretical models to practical implementation. Overall, this study demonstrates that hybrid ionanofluids are a promising class of next-generation working fluids that offer significant advantages over conventional nanofluids for advanced thermal system design.

Author contributions

Abanti Datta: Conceptualization, Methodology, Validation, Formal analysis, Investigation, Supervision, Data Curation, Writing-Original Draft, **Arka Banerjee:** Conceptualization, Methodology, Validation, Formal analysis, Investigation, Writing-Original Draft, Writing-Review & Editing **Sayantan Mukherjee:** Formal analysis, Methodology, Investigation, Resources, Conceptualization, Writing-Review & Editing."

Conflicts of interest

The authors assert that they possess no identifiable competing financial interests or personal ties that may have seemingly influenced the work presented in this study.

Acknowledgements

We sincerely thank all individuals and institutions whose support and insights contributed to the completion of this work.

References

1. Sidik NAC, Adamu IM, Jamil MM, Kefayati GHR, Mamat R, Najafi G. Recent progress on hybrid nanofluids in heat transfer applications: A comprehensive review. Int Commun Heat Mass Transf. 2016;78:68-79. https://doi.org/10.1016/j.icheatmasstransfer.2016.08.019
2. Huminic G, Huminic A. Hybrid nanofluids for heat transfer applications - A state-of-the-art review. Int J Heat Mass Transf. 2018;125:82-103. https://doi.org/10.1016/j.ijheatmasstransfer.2018.04.059
3. Maxwell JC. A Treatise on Electricity and Magnetism. Oxford: University of Oxford; 1873.
4. Hamilton RL, Crosser OK. Thermal conductivity of heterogeneous two-component systems. Ind Eng Chem Fund. 1962;1(3):187-191. https://doi.org/10.1021/i160003a005
5. Choi SUS, Eastman JA. Enhancing thermal conductivity of fluids with nanoparticles. ASME Fluids Eng Div. 1995;231:99-106. https://doi.org/10.1115/IMECE1995-0926
6. Sarkar J, Ghosh P, Adil A. A review on hybrid nanofluids: Recent research, development and applications. Renew Sustain

Energy Rev. 2015;43:164-177. https://doi.org/10.1016/j.rser.2014.11.023
7. Sundar LS, Sharma KV, Singh MK, Sousa ACM. Hybrid nanofluids preparation, thermal properties, heat transfer and friction factor-A review. Renew Sustain Energy Rev. 2017;68:185-198. https://doi.org/10.1016/j.rser.2016.09.108
8. Babu JR, Kumar KK, Rao SS. State-of-art review on hybrid nanofluids. Renew Sustain Energy Rev. 2017;77:551-565. https://doi.org/10.1016/j.rser.2017.04.040
9. Rohni AM, Ahmad S, Ismail AIM, Pop I. Boundary layer flow and heat transfer over an exponentially shrinking vertical sheet with suction. Int J Therm Sci. 2013;64:264-272. https://doi.org/10.1016/j.ijthermalsci.2012.08.016
10. Sathish Kumar M, Sandeep N, Rushi Kumar B, Dinesh PA. A comparative analysis of magnetohydrodynamic non-Newtonian fluids flow over an exponential stretched sheet. Alex Eng J. 2018;57(3):2093-2100. https://doi.org/10.1016/j.aej.2017.06.002
11. Merkin JH, Najib N, Bachok N, Ishak A, Pop I. Stagnation-point flow and heat transfer over an exponentially stretching/shrinking cylinder. J Taiwan Inst Chem Eng. 2017;74:65-72. https://doi.org/10.1016/j.jtice.2017.02.008
12. Ur Rehman F, Nadeem S, Ur Rehman H, Ul Haq R. Thermophysical analysis for three-dimensional MHD stagnation-point flow of nanomaterial influenced by an exponential stretching surface. Results Phys. 2018;8:316-323. https://doi.org/10.1016/j.rinp.2017.12.026
13. Ghosh S, Mukhopadhyay S. Flow and heat transfer of nanofluid over an exponentially shrinking porous sheet with heat and mass fluxes. Propuls Power Res. 2018;7(3):268-275. https://doi.org/10.1016/j.jppr.2018.07.004
14. Lund LA, Omar Z, Khan I. Quadruple solutions of mixed convection flow of magnetohydrodynamic nanofluid over exponentially vertical shrinking and stretching surfaces: Stability analysis. Comput Methods Programs Biomed. 2019;182:105044. https://doi.org/10.1016/j.cmpb.2019.105044
15. Manjunatha S, AmmaniKuttan B, Jayanthi S, Chamkha A, Gireesha BJ. Heat transfer enhancement in the boundary layer flow of hybrid nanofluids due to variable viscosity and natural convection. Heliyon. 2019;5(4):e01469. https://doi.org/10.1016/j.heliyon.2019.e01469
16. Bumataria RK, Chavda NK, Panchal H. Current research aspects in mono and hybrid nanofluid based heat pipe technologies. Heliyon. 2019;5(5):e01627. https://doi.org/10.1016/j.heliyon.2019.e01627
17. Huminic G, Huminic A, Dumitrache F, Fleaca C, Morjan I. Study of the thermal conductivity of hybrid nanofluids: Recent research and experimental study. Powder Technol. 2020;367:347-357. https://doi.org/10.1016/j.powtec.2020.03.052
18. Bhattacharyya K. Boundary layer flow and heat transfer over an exponentially shrinking sheet. Chin Phys Lett. 2011;28(7):074701. https://doi.org/10.1088/0256-307X/28/7/074701
19. Waini I, Ishak A, Pop I. Mixed convection flow over an exponentially stretching/shrinking vertical surface in a hybrid nanofluid. Alex Eng J. 2020;59(3):1881-1891. https://doi.org/10.1016/j.aej.2020.05.030
20. Dero S, Rohni AM, Saaban A. Stability analysis of Cu-C6H9NaO7 and Ag-C6H9NaO7 nanofluids with effect of viscous dissipation over stretching and shrinking surfaces using a single-phase model. Heliyon. 2020;6(4):e03510.
21. Khashi'ie NS, Arifin NM, Pop I, Nazar R, Hafidzuddin EH, Wahi N. Flow and heat transfer past a permeable power-law deformable plate with orthogonal shear in a hybrid nanofluid. Alex Eng J. 2020;59(3):1869-1879. https://doi.org/10.1016/j.aej.2020.05.029
22. Zainal NA, Nazar R, Naganthran K, Pop I. Heat generation/absorption effect on MHD flow of hybrid nanofluid over bidirectional exponential stretching/shrinking sheet. Chin J Phys. 2021;69:118-133. https://doi.org/10.1016/j.cjph.2020.12.002
23. Rao Y. Nanofluids: Stability, phase diagram, rheology and applications. Particuology. 2010;8(6):549-555. https://doi.org/10.1016/j.partic.2010.08.004
24. Ribeiro APC, Lourenço MJV, Nieto de Castro C, Hardacre C. Thermal conductivity of 'Bucky Gels'. In: Proceedings of the Conference on Molten Salts and Ionic Liquids (EUCHEM2008). Copenhagen; 2008:24-29.
25. Nieto de Castro C. Thermophysical properties of ionic liquids: Do we know how to measure them accurately? J Mol Liq. 2010;156(1):10-17. https://doi.org/10.1016/j.molliq.2010.06.007
26. Pak BC, Cho YI. Hydrodynamic and heat transfer study of dispersed fluids with submicron metallic oxide particles. Exp Heat Transf. 1998;11(2):151-170. https://doi.org/10.1080/08916159808946559
27. Xuan Y, Roetzel W. Conceptions for heat transfer correlation of nanofluids. Int J Heat Mass Transf. 2000;43(19):3701-3707. https://doi.org/10.1016/S0017-9310(99)00369-5
28. Titan CP, Morshed AKMM, Fox E, Khan AJ. Enhanced thermophysical properties of NEILs as heat transfer fluids for solar thermal applications. Appl Therm Eng. 2017;110:1-9. https://doi.org/10.1016/j.applthermaleng.2016.08.004
29. Minea AA, El-Maghlany WM. Influence of hybrid nanofluids on the performance of parabolic trough collectors in solar thermal systems: Recent findings and numerical comparison. Renew Energy. 2018;120:350-364. https://doi.org/10.1016/j.renene.2017.12.093
30. Chereches EI, Viswanatha Sharma K, Minea AA. A numerical approach in describing ionanofluids behavior in laminar and turbulent flow. Continuum Mech Thermodyn. 2018;31(2):497-506. https://doi.org/10.1007/s00161-018-0634-x
31. Minea AA, El-Maghlany WM. Natural convection heat transfer utilizing ionic nanofluids with temperature-dependent thermophysical properties. Chem Eng Sci. 2017;174:13-24. https://doi.org/10.1016/j.ces.2017.08.028
32. Minea AA, Moldoveanu MG, Dodun O. Thermal conductivity enhancement by adding nanoparticles to ionic liquids. Solid State Phenom. 2017;261:121-126. https://doi.org/10.4028/www.scientific.net/SSP.261.121
33. Asghar A, Dero S, Lund LA, Shah Z, Alshehri MH, Vrinceanu N. Slip effects on magnetized radiatively hybridized ferrofluid flow with acute magnetic force over shrinking/stretching surface. Open Phys. 2024;22:20240052. https://doi.org/10.1515/phys-2024-0052
34. Asghar A, Teh YY, Javed Iqbal M, Ali L. Thermal characterization of hybrid nanofluid with impact of convective boundary layer flow and Joule heating law: Dual solutions case study. Mod Phys Lett B. 2024;38:2450158. https://doi.org/10.1142/S0217984924501586
35. Soomro AM, Lund LA, Asghar A, Bonyah E, Shah Z, Garalleh HA. Magnetized Casson SA-hybrid nanofluid flow over a permeable moving surface with stability analysis. Int J Thermofluids. 2024;21:100555. https://doi.org/10.1016/j.ijft.2023.100555
36. Asghar A, Hanafy H, Fadhel MA, Lund LA, Khan SU, Tlili I. Darcy-Forchheimer radiative flow of a hybrid nanofluid with velocity mass flux and thermal stability. J Porous Media. 2025;28(5):71-87. https://doi.org/10.1615/JPorMedia.2024051851
37. Asghar A, Nangraj AR, Dero S, Shah NA, Lund LA. Dual solutions for the Darcy-Forchheimer porous medium with convective heat transfer effect on rotating hybrid nanofluid. Z Angew Math Mech. 2025;105:e70046. https://doi.org/10.1002/zamm.70046
38. Asghar A, Ying TY, Lund LA, Shah Z, Vrinceanu N, Islam S. Radiative porosity sodium alginate hybrid nanofluid flow over an exponential stretching/shrinking surface: Dual solutions. Nano-Struct Nano-Objects. 2025;42:101463. https://doi.org/10.1016/j.nanoso.2025.101463

39. Asghar A, Govindarajoo MV, Ara H, Zaimi K, Ying TY, Lund LA. Effect of water-based alumina-copper MHD hybrid nanofluid on a power-law form stretching/shrinking sheet with Joule heating and slip condition: Dual solutions study. CFD Lett. 2024;17(3):119-135. https://doi.org/10.37934/cfdl.17.4.119135
40. Fadhel MA, Asghar A, Lund LA, Shah Z, Vrinceanu N, Tirth V. Dual numerical solutions of Casson SA-hybrid nanofluid toward a stagnation point flow over stretching/shrinking cylinder. Nanotechnol Rev. 2024;13:20230191. https://doi.org/10.1515/ntrev-2023-0191
41. Ramya D, Rao JA, Shravani I. Numerical Simulation of MHD Boundary Layer Stagnation Flow of Nanofluid over a Stretching Sheet with Slip and Convective Boundary Conditions. Int J Nanosci Nanotechnol. 2020;16(2):103-115.
42. Peiravi MM, Ashabi A. Magneto Effects on Fe3O4 Nanoparticles through the Triangular and Rectangular Baffles on Thread Stretching Surface for Rotary Seals in Computer Hardware. Int J Nanosci Nanotechnol. 2022;18(3):143-156.
43. Devi SSU, Devi SPA. Numerical investigation of three-dimensional hybrid Cu-Al_2O_3/water nanofluid flow over a stretching sheet with effecting Lorentz force subject to Newtonian heating. Can J Phys. 2016;94(5):490-496. https://doi.org/10.1139/cjp-2015-0799
44. Waini I, Ishak A, Pop I. Hybrid nanofluid flow induced by an exponentially shrinking sheet. Chin J Phys. 2019;60:125-133.
45. Ghosh S, Mukhopadhyay S. Stability analysis for model-based study of nanofluid flow over an exponentially shrinking permeable sheet in presence of slip. Neural Comput Appl. 2020;32(11):7201-7211. https://doi.org/10.1007/s00521-019-04221-w
46. Mukhopadhyay S, Andersson HI. Effects of slip and heat transfer analysis of flow over an unsteady stretching surface. Heat Mass Transf. 2009;45(11):1447-1452. https://doi.org/10.1007/s00231-009-0516-7
47. Eid MR, Nafe MA. Thermal conductivity variation and heat generation effects on magneto-hybrid nanofluid flow in a porous medium with slip condition. Waves Random Complex Media. 2020;32(6):2835-2859. https://doi.org/10.1080/17455030.2020.1810365
48. Hayat T, Nadeem S. Heat transfer enhancement with Ag-CuO/water hybrid nanofluid. Results Phys. 2017;7:2317-2324. https://doi.org/10.1016/j.rinp.2017.06.034
49. Merkin JH. On dual solutions occurring in mixed convection in a porous medium. J Eng Math. 1986;20(2):171-179. https://doi.org/10.1007/BF00042775
50. Weidman PD, Kubitschek DG, Davis AMJ. The effect of transpiration on self-similar boundary layer flow over moving surfaces. Int J Eng Sci. 2006;44(11-12):730-737. https://doi.org/10.1016/j.ijengsci.2006.04.005
51. Yan L, Dero S, Khan I, Mari IA, Baleanu D, Nisar KS, et al. Dual solutions and stability analysis of magnetized hybrid nanofluid with Joule heating and multiple slip conditions. Processes. 2020;8(3):332. https://doi.org/10.3390/pr8030332
52. Chereches EI, Minea AA. Experimental evaluation of electrical conductivity of ionanofluids based on water-[C_2mim][CH_3SO_3] ionic liquids mixtures and alumina nanoparticles. J Therm Anal Calorim. 2021;145(6):3151-3157. https://doi.org/10.1007/s10973-020-09925-z
53. Datta A, Kumar S, Halder P. Heat transfer and thermal characteristics effects on moving plate impinging from Cu-water nanofluid jet. J Therm Sci. 2020;29(1):182-193. https://doi.org/10.1007/s11630-019-1107-7
54. Datta A, Halder P. Thermal efficiency and hydraulic performance evaluation on Ag-Al_2O_3 and SiC-Al_2O_3 hybrid nanofluid for circular jet impingement. Arch Thermodyn. 2021;42(1):163-182. https://doi.org/10.24425/ather.2021.136953
55. Brinkman HC. The viscosity of concentrated suspensions and solutions. J Chem Phys. 1952;20(4):571-581. https://doi.org/10.1063/1.1700493
56. Kierzenka J, Shampine LF. A BVP solver based on residual control and the MATLAB PSE. ACM Trans Math Softw. 2001;27(3):299-316. https://doi.org/10.1145/502800.502801
57. Hafidzuddin MEH, Nazar R, Arifin NM, Pop I. Boundary layer flow and heat transfer over a permeable exponentially stretching/shrinking sheet with generalized slip velocity. J Appl Fluid Mech. 2016;9(4):2025-2036. https://doi.org/10.18869/acadpub.jafm.68.235.24834
58. Ishak A. MHD boundary layer flow due to an exponentially stretching sheet with radiation effect. Sains Malays. 2011;40(4):391-395.
59. Magyari E, Keller B. Heat and mass transfer in the boundary layers on an exponentially stretching continuous surface. J Phys D Appl Phys. 1999;32(5):577-585. https://doi.org/10.1088/0022-3727/32/5/012
60. Bidin B, Nazar R. Numerical solution of the boundary layer flow over an exponentially stretching sheet with thermal radiation. Eur J Sci Res. 2009;33(4):710-717.
61. Tiwari RK, Das MK. Heat transfer augmentation in a two-sided lid-driven differentially heated square cavity utilizing nanofluids. Int J Heat Mass Transf. 2007;50(9-10):2002-2018. https://doi.org/10.1016/j.ijheatmasstransfer.2006.09.034